The volume dependence of the magnetization and NMR of Fe_4N and Mn_4N

1994 J. Phys.: Condens. Matter 6 1779

(http://iopscience.iop.org/0953-8984/6/9/019)

J. Phys.: Condens. Matter 6 (1994) 1779–1790. Printed in the UK

The volume dependence of the magnetization and NMR of Fe_4N and Mn_4N

J S Lord†, J G M Armitage†, P C Riedi†, S F Matar‡ and G Demazeau‡

† J F Allen Laboratories, Department of Physics and Astronomy, University of St Andrews, Fife KY16 9SS, UK

‡ Laboratoire de Chemie du Solide du CNRS, Université Bordeaux-I, 351 Course de la Libération, 33405 Talence, France

Received 1 November 1993

Abstract. The forced volume magnetostriction and the NMR of ferromagnetic Fe_4N and ferrimagnetic Mn_4N have been measured in the ordered state. At 4.2 K the magnetization (σ) per unit mass and the effective field (H_I) at the nucleus of the Fe(I) site of Fe_4N are found to change with pressure such that $\partial \ln \sigma / \partial P \simeq \partial \ln |H_I| / \partial P < 0$, while for Mn_4N $\partial \ln \sigma / \partial P \simeq 6\partial \ln |H_I| / \partial P > 0$. The result for Mn_4N is interpreted as showing that the magnitude of the small (negative) moment on the Mn(II) site decreases more rapidly under pressure than does the large Mn(I) moment. The value of $\partial \ln |H_I| / \partial P$ for Mn_4N was found to be a strong function of temperature such that $\partial \ln T_N / \partial P \simeq 5.2$ Mbar^{-1}. An analysis of the Mn_4N NMR data suggests that the discrepancy between the calculated (spin) and measured moment at the Mn(I) site may be due to a small orbital moment at that site.

1. Introduction

The transition metal nitrides M_4N, where M is Fe or Mn, are expanded lattice metals whose magnetic properties are of interest in both pure and applied physics. The introduction of N to the M lattice leads to an $\sim 30\%$ increase in volume and to two inequivalent M sites, M(I) and M(II). The M(I) site carries a large moment with little interaction with N while there is strong bonding between M(II) and N. The M(I)–M(II) interaction is ferromagnetic for Fe_4N and ferrimagnetic for Mn_4N. The M_4N compounds have been extensively studied by magnetization [1–3], neutron scattering [1–3], NMR [4–6] and Mössbauer techniques [7, 8] over the last 30 years and are of renewed interest because of the potential use of derivatives of Fe_4N in magnetic recording [7–9] and their relation to the invar effect [10, 11].

In view of the large lattice expansion associated with the formation of M_4N, and the very different bonding of the M(I) and M(II) sites, it is particularly interesting to investigate their magnetic properties as a function of pressure. Early theories of M_4N assumed an ionic model but the more recent theoretical treatments discussed in section 3 [12–15] emphasize the metallic nature of M_4N. It would therefore be expected that the magnetization of Fe_4N would decrease under pressure while that of Mn_4N would increase because the small (negative) moment on the M(II) site should be more sensitive to pressure than that on the M(I) site. In the present paper we show that the magnetization (σ) per unit mass of Fe_4N and Mn_4N under pressure does behave as predicted theoretically but the pressure derivatives are quite small, showing that the large moment on the M(I) site of Mn_4N in particular is insensitive to a small change of volume.

0953-8984/94/091779+12$19.50

The ^{57}Fe NMR of Fe_4N at the Fe(I) and Fe(II) sites has been measured as a function of pressure up to 9 kbar at 4.2 K. The logarithmic pressure derivative $\partial \ln|H|/\partial P$ of the magnitude of the effective magnetic field at the nucleus, was found to be nearly equal to $\partial \ln\sigma/\partial P$ for both sites. The ^{55}Mn NMR of the Mn(I) and Mn(II) sites of Mn_4N and of satellite lines due to one N vacancy, $Mn(I_a)$, and two N vacancies, $Mn(I_b)$, has been measured as a function of temperature and pressure from 4.2 K to room temperature. The strong temperature dependence of $\partial \ln|H_I|/\partial P$ is attributed to an increase of the Néel temperature under pressure, which cannot be measured in our equipment directly, by ~ 4 K kbar^{-1}. The value of $\partial \ln|H_I|/\partial P$ will be shown to be consistent with a model in which only the Mn(II) moment changes appreciably with pressure. An analysis of the frequency of the $Mn(I_a)$ satellite line and of the value of $\partial \ln|H_I|/\partial P$ for Mn(I) was found to lead to the same contributions to the effective field at the Mn(I) site, provided that the magnitude of the moment at the Mn(II) site next to an N vacancy increases by $1\mu_B$ as first suggested from neutron scattering measurements [1]. The value found for the effective field at the Mn(1) site is not consistent with a spin only moment at that site, but is understandable if there is also an orbital moment of $\sim 0.4\mu_B$. Since spin only calculations [12] have indeed found a lower moment than that measured by neutron diffraction, this possibility deserves further investigation.

2. Magnetic structure

The structure of M_4N is of the perovskite type, which can be viewed as a face centred cubic M structure with an N at the cube centre. There are two crystallographically inequivalent M sites, one, M(I), at the cube corner, and the other, M(II), at the cube face. The effect of the inclusion of N is to increase the volume of the material so that for Fe_4N the lattice constant is 10% larger than that of γ Fe. The moments at the two M sites are very different in magnitude (table 1). The low moment at the M(II) site is considered to arise from a stronger interaction with N than occurs at the M(I) site because the M(I)–N distance is $\sqrt{3}$ times that of M(II)–N.

The magnetic structure of Fe_4N is ferromagnetic but Mn_4N is more complicated (table 1). The basic interaction between Mn(I) and Mn(II) is ferrimagnetic, but there is a small temperature dependent triangular magnetic component at the Mn(II) sites [3]. The moments on the two Mn sites change differently with temperature. By 300 K the Mn(I) moment has decreased by about 10% from the value at 0 K while that of Mn(II) is almost unchanged [2, 3]. The effect of vacancies at the N sites in the Mn_4N structure has been analysed by Takei *et al* [1] using neutron diffraction and magnetization measurements. They concluded that there was little change in the moment at the Mn(I) site next to an N vacancy but that the Mn(II) moment changed from -0.90 to $-1.9\mu_B$. An N vacancy leads to a satellite line in the ^{55}Mn NMR of Mn_4N and it will be shown below that the difference between the frequencies of the main and satellite lines tends to support the conclusion of Takei *et al* that the moment of Mn(II) sites next to an N vacancy increases in magnitude.

3. Computed ground state of M_4N

The early attempts to understand the properties of M_4N in terms of an ionic model were unsuccessful (see [12] and [8] for reviews). Matar *et al* [12] used the augmented spherical wave (ASW) method to calculate the properties of M_4N. They showed that $Mn_4(Fe_4)N$ was

Table 1. The moments measured by neutron diffraction experiments at low temperature [1–3] and the calculated values [12] for Fe_4N and Mn_4N. There is also a small triangular magnetic component at the Mn(II) sites [3]. The $Mn(II_a)$ site is the nearest neighbour of an N vacancy.

	Experiment	Calculation
Fe(I)	3.00	2.98
Fe(II)	2.00	1.79
Mn(I)	3.85	3.23
Mn(II)	−0.90	−0.80
$Mn(II_a)$	−1.90	—

ferri(ferro)magnetic and emphasized the covalent nature of the bonding between N and M(II) and the isolation of the M(I) site. Kuhnen *et al* [8] made a linear muffin tin orbital (LMTO) calculation, which showed a charge transfer from Fe(I) and N to Fe(II) sites, in agreement with their Mössbauer measurements of the isomer shifts at the two sites. Kuhnen *et al* stressed the metallic character of Fe_4N, with a common d band for Fe(I), Fe(II) and N, but concluded that the moments were essentially localized at the Fe(I) and Fe(II) sites. Tagawa and Motizuki [13] have made an augmented plane wave (APW) calculation for Mn_4N and Ishida and Kitawatse [14] an LMTO calculation for Fe_4N whose essential features are in agreement with [8].

The values of the spin moments at the Fe(I), Fe(II) and Mn(II) sites given by the above calculations were all in good agreement with the neutron data and support a model in which the greatly reduced moment on the M(II) site, compared to that of M(I), arises from the strong N–M(II) interaction. There is a large discrepancy between the measured moment at the Mn(I) site ($3.85\mu_B$) and the calculated spin values of 3.2–$3.0\mu_B$, which may be due to an orbital moment at this site, as discussed below.

Siberchicot and Matar [15] extended the ASW calculation of Matar *et al* [12] to calculate the magnetic moments of Mn_4N as a function of pressure. A weak but significant increasing charge transfer from N to Mn(II) was found to occur with increasing volume. The absolute magnitudes of the moments at Mn(I) and Mn(II) sites decreased with pressure but the moment at the Mn(II) site was found to be far more pressure sensitive and lead to an overall increase of the net magnetization, in agreement with the conclusions of NMR and magnetostriction measurements discussed below.

Matar *et al* [12] and Kuhnen *et al* [8] both calculated the contact interaction at the Fe sites of Fe_4N and obtained values of the effective field in good agreement with experiment. Matar *et al* also calculated the contact interaction contribution to the effective field at the Mn sites of Mn_4N, but the values found, Mn(I) ~ -50 kG, Mn(II) ~ 30 kG, were, as discussed further in section 5.2, in poor agreement with experiment (table 2).

4. Experimental details

4.1. Sample preparation

4.1.1. Fe_4N. Divalent iron oxalate, with particle sizes of $\sim 1\mu$m, was used as a precursor to prepare Fe_4N. The oxalate was decomposed under a stream of hydrogen–ammonia gas mixture with a ratio $NH_3/H_2 \simeq 1$ at 400 °C for 5 h (1 h at 120 °C and 4 h at 400 °C). The reaction is of the solid–gas type and is hence carried out in the so-called fluidized bed reactor, which ensured a more intimate contact between solid particles of the precursor and the reacting gas mixture. After the reaction the furnace was left to cool down under

Table 2. The NMR frequencies ν (MHz), and equivalent effective fields H (kG), for the ^{57}Fe NMR of Fe_4N and the ^{55}Mn NMR of Mn_4N at 4.2 K and room temperature. The first entry for Mn(I) is for the sample whose spectrum is shown in the upper part of figure 4 and the others are for the sample whose spectrum is shown in the lower part.

	$\nu(H)_{4.2}$	$\nu(H)_{RT}$	$\nu_{RT}/\nu_{4.2}$
Fe(I)	51.0(−369)	—(−341) [8]	0.92
Fe(II)	32.3(−234)	—(−217) [8]	0.93
Mn(I)	133.8(−126.8)	117.1(−111.0)	0.875
Mn(I)	134.1(−127.1)	117.9(−111.7)	0.879
$Mn(I_a)$	115.1(−109.1)	104.8(−99.3)	0.911
$Mn(I_b)$	99.8(−94.5)	94.5(−89.5)	0.947
Mn(II)	20–65	20–60	—

a reduced rate of gas flow. The resulting magnetic product was then collected in toluene, which traps adsorbed hydrogen, rapidly washed with acetone, and dried.

4.1.2. Mn_4N. As MnO readily formed when a solid–gas reaction of the type described above was attempted to prepare Mn_4N from similar precursors or from the finely divided metal, another procedure was adopted to prepare Mn_4N in the solid state. The procedure starts with the homogenization of powders of Mn_2N and Mn in an agate mortar. The powder is then introduced into a silica tube and sealed under vacuum. The reaction was carried out for $\sim$ 12 h at 650 °C.

The x-ray diffraction patterns of the nitride powders were characteristic of pure Fe_4N and Mn_4N. The lattice parameter of Fe_4N, 3.797 ± 0.003 Å, was found to agree with earlier measurements, but systematically lower values of the lattice parameter of the Mn_4N samples were obtained by the solid state reaction procedure: 3.852 ± 0.003 Å as compared to 3.865 Å [1]. This difference is indicative of the presence of N vacancies, i.e. $Mn_4N_{1-\delta}$ with $\delta \simeq 0.1$, see section 5.2 below.

4.2. Experimental techniques

The forced magnetostriction at 4.2 K was measured on thin discs of pressed powder using a capacitance technique, which has already been described [16]. The field of up to 12 T was applied in the plane of the disc and the change in length parallel and perpendicular to the field recorded.

The ^{55}Mn NMR spectrum of Mn_4N and the ^{57}Fe NMR of Fe_4N were measured as functions of pressure up to 9 kbar at 4.2 K using a computer controlled phase coherent swept frequency spin echo spectrometer [17]. The powder samples were immersed in liquid and pressure applied at room temperature to a Be–Cu lock cell. The pressure was measured using a calibrated semiconductor pressure transducer. The small nuclear moment and low isotopic concentration (2%) of ^{57}Fe in natural Fe led to weak NMR signals that could only be observed at low temperature, but measurements of the effective fields at the nucleus at room temperature have been reported for Fe_4N using the Mössbauer effect [8].

The strong ^{55}Mn NMR signal from Mn_4N could easily be observed up to room temperature. The spectrum was found to be sample dependent because slight variations from the nominal Mn_4N composition led to N vacancies and satellite lines on the Mn(I) NMR. The temperature dependence of the main Mn(I) line and of the satellite line due to one N vacancy, $Mn(I_a)$, and two N vacancies $Mn(I_b)$, was measured from 4.2 K to room temperature in a gas flow cryostat by allowing the sample temperature to drift slowly while

repeated spin echoes were captured and analysed by the computer. The spin echo was detected in two channels with $\pi/2$ phase difference between the reference waveforms and resolved into amplitude and phase components. At exact resonance the phase (ϕ) will be constant across the echo; otherwise $d\phi/dt$ is equal to the frequency offset and therefore the frequency (ν_0) for resonance can be calculated. The computer now sets the frequency of the frequency synthesizer to ν_0 and continues to track the NMR frequency as a function of temperature. This method, which we have not seen reported before, gave results in good agreement with measurements made at fixed temperature and will be published in detail elsewhere.

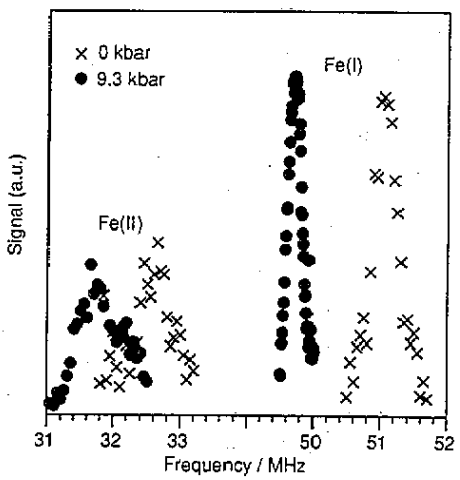

Figure 1. The ^{57}Fe NMR spectrum of Fe_4N under atmospheric pressure and 9.3 kbar at 4.2 K.

5. Discussion

5.1. Fe_4N

The ^{57}Fe NMR of Fe_4N provides weak signals and was only measured at and below 4.2 K. The main feature of the spectrum (figure 1) is that the width of the Fe(II) line is a factor of three greater than that of Fe(I). Since ^{57}Fe has spin $\frac{1}{2}$, the width of the spectrum is due only to the distribution of effective magnetic fields at the two sites and shows, as expected, the greater sensitivity of the Fe(II) site to vacancies on the N sites. The frequencies of the two lines at 4.2 K (table 2) combined with room temperature Mössbauer measurements [8] show that the effective field at both sites has decreased by a factor of 0.92 between 4.2 K and room temperature. The pressure dependence of the effective field at the two Fe sites of Fe_4N is shown in figures 1 and 2. Due to the width of the Fe(II) line, and the small change of frequency under a pressure of 9 kbar, the accuracy of the value of $\partial \ln \nu/\partial P$ is only about ±50% (table 3). As indicated in figure 2, it is quite possible that the value of $\partial \ln \nu/\partial P$ for Fe(I) is identical to that of Fe(II).

The forced linear magnetostriction of Fe_4N is shown in figure 3. Apart from the usual rapid change of length with field until the domain structure has been removed, see, e.g., [16],

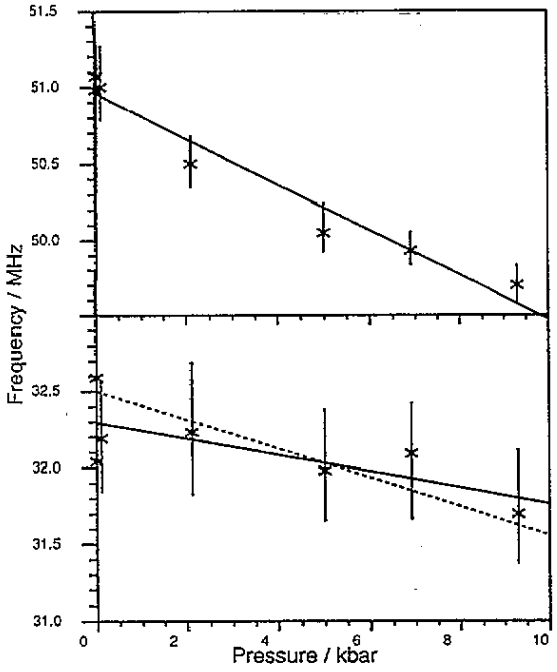

Figure 2. The pressure dependence of the ^{57}Fe NMR frequency (ν) of Fe_4N at 4.2 K. The full lines are linear least-squares fits to the data from the Fe(I) site (top) and Fe(II) site (bottom). The dotted line shows the slope for the Fe(II) NMR frequency if the value of $\partial \ln \nu / \partial P$ were the same as for the Fe(I) site.

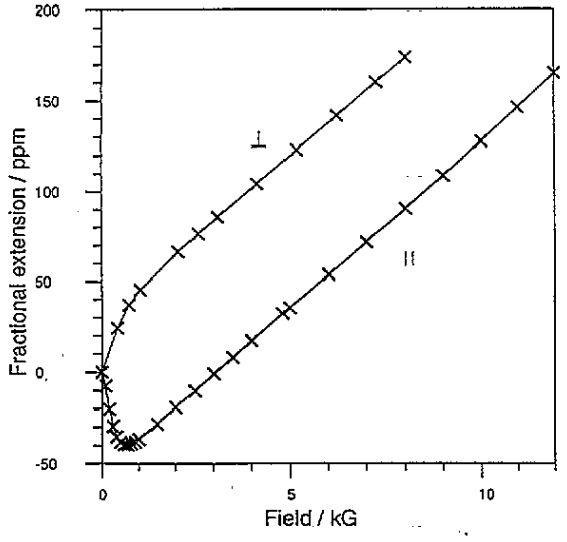

Figure 3. The forced linear magnetostriction of a diameter of a disc of pressed powder of Fe_4N measured parallel (||) and perpendicular ($\perp$) to the field direction with the field in the plane of the disc.

the forced magnetostriction is seen to be linear with field. The value of the change in length parallel to the field, $\partial \ln l_{\parallel}/\partial H = 1.84$ ppm kG^{-1} is remarkably close to that perpendicular to it, $\partial \ln l_{\perp}/\partial H = 1.80$ ppm kG^{-1} as was also found for the related compound $NiFe_3N$ [11]. The value of $\partial \ln V/\partial B$ is 5.44 ppm kG^{-1}. Using the thermodynamic Maxwell relation $(\partial \sigma_T/\partial P) = -(1/\rho)(\partial \ln V/\partial H)_T$, where σ_T is the magnetization per unit mass at temperature T and ρ the density, we deduce that $\partial \ln \sigma_0/\partial P = -3.6$ Mbar^{-1}.

The magnetization and the magnitudes of the effective field at the Fe(I) and Fe(II) sites therefore all decrease with pressure at low temperature, as expected for a band ferromagnet,

Table 3. The pressure dependence of the magnetization (σ) per unit mass and the magnitude of the effective field (H) at the ^{57}Fe nucleus of Fe_4N and ^{55}Mn nucleus of Mn_4N at 4.2 K. The units are $Mbar^{-1}$.

	$\partial \ln \sigma / \partial P$	$\partial \ln \lvert H \rvert / \partial P$
Fe_4N	-3.6 ± 0.3	—
Fe(I)	—	-2.9 ± 0.3
Fe(II)	—	-1.7 ± 0.9
Mn_4N	~1	—
Mn(I)	—	0.110 ± 0.005
$Mn(I_a)$	—	0.21 ± 0.05
$Mn(I_b)$	—	-0.05 ± 0.05

but the magnitude of $\partial \ln \sigma_0 / \partial P$ is small and comparable to $\partial \ln |H| / \partial P$, supporting the view of Kuhnen *et al* [8] that the Fe moments are essentially localized. The magnitude of $\partial \ln \sigma_0 / \partial P$ for Fe_4N is about 10 times greater than for Fe but some 30 times smaller than for a weak itinerant ferromagnet such as $ZrZn_2$ or $Y(Co_{1-x}Al_x)_2$ [18]. It should be remembered that the most important quantity is $\partial \ln \sigma_0 / \partial \ln V$, which has the value of 0.5 for Fe and 30 for $ZrZn_2$. The value of $\partial \ln \sigma_0 / \partial \ln V$ is equal to $-B_0 \partial \ln \sigma_0 / \partial P$, where B_0 is the low-temperature bulk modulus, but at present B_0 is not known for Fe_4N.

5.2. Mn_4N

The forced magnetostriction of Mn_4N at 4.2 K was found to be sample dependent, and did not show a linear variation with field even at 12 T. It was therefore only possible to obtain an estimate that $\partial \ln V / \partial H \sim -1.0$ ppm T^{-1} and hence that $\partial \ln \sigma_0 / \partial P \sim +1$ $Mbar^{-1}$. This small positive value is in agreement with a recent calculation of the magnetization of Mn_4N as a function of lattice constant [15], which shows that the moment on the rather isolated Mn(I) site is nearly independent of pressure while the magnitude of the (negative) moment on the Mn(II) decreases under pressure.

The ^{55}Mn NMR spectrum at 4.2 K shows (figure 4) a narrow line near 134 MHz, which is attributed to the Mn(I) site, a broad distribution in the range 20–60 MHz due to Mn(II) and lines near 115 MHz, for $Mn(I_a)$, and 100 MHz, $Mn(I_b)$, attributed to an Mn(I) site with one or two N vacancies as near neighbours respectively. The intensity of the $Mn(I_a)$ and $Mn(I_b)$ lines can therefore be used to monitor how close a sample is to the nominal Mn_4N composition. The exact shape and intensity of the Mn(II) spectrum is difficult to determine because of its width, which is due to a combination of electric field gradients, since the nuclear spin of ^{55}Mn is $\frac{5}{2}$, and the sensitivity of the moment at the Mn(II) site to N vacancies.

The Mn(I) site has cubic symmetry and therefore only a magnetic interaction leading to the narrow line shown in figure 4, but a N vacancy breaks the cubic symmetry and would be expected to lead to an appreciable quadrupole interaction at the $Mn(I_a)$ site. This interaction is not sufficient to split the $Mn(I_a)$ line into five lines but does lead to an oscillatory decay of the spin echo as a function of pulse spacing (figure 5) as first demonstrated by Abe *et al* [19]. The period of oscillation (τ) is related to the quadrupole splitting ($\Delta \nu_q$) by the relation $\tau \Delta \nu_q = 1$.

An analysis of the spin echo decay shown in figure 5 for the $Mn(I_a)$ site, using the linear prediction by singular-value decomposition (LPSVD) technique [20], showed that there were two frequencies present, $\Delta \nu_q = 262$ and 228 kHz, with an intensity ratio of 2:1. Due to the presence of domain walls in the material it is not clear how to relate these values to the exact

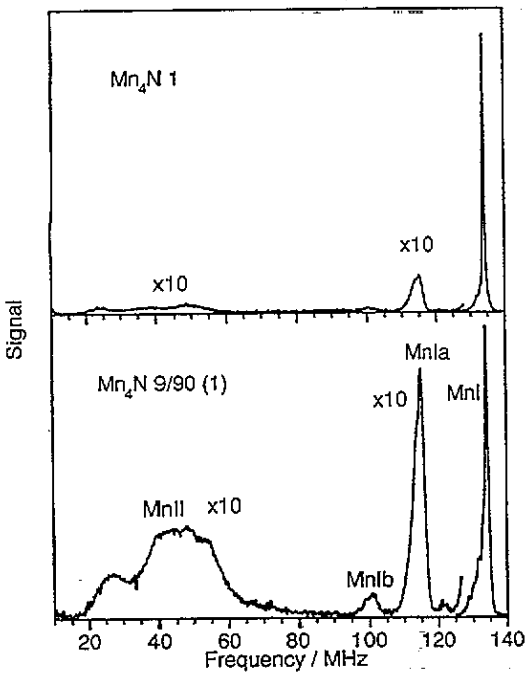

Figure 4. The ^{55}Mn NMR spectrum of two samples of Mn_4N at 4.2 K showing lines from the Mn(I) and Mn(II) sites and satellite lines of the Mn(I) NMR due to one, $Mn(I_a)$, or two, $Mn(I_b)$, nearest-neighbour N vacancies.

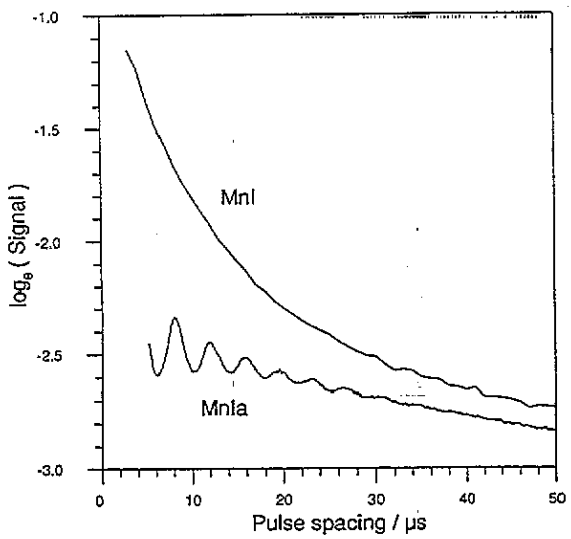

Figure 5. The spin echo decay at 4.2 K of the ^{55}Mn NMR of Mn_4N at the Mn(I) and $Mn(I_a)$ sites.

electric field gradient (EFG) at the nuclei, but they will provide a check on first-principles calculations of the EFG at present in progress [23].

The temperature dependence of the Mn(I), $Mn(I_a)$ and $Mn(I_b)$ frequencies is shown in figure 6. The width of the Mn(II) distribution precludes any determination of its temperature dependence. It will be seen that the Mn(I) line shows the strongest dependence on temperature. This is consistent with the neutron data [2, 3], which show that the moment at the Mn(I) site at room temperature is about 0.9 times that at low temperature while that

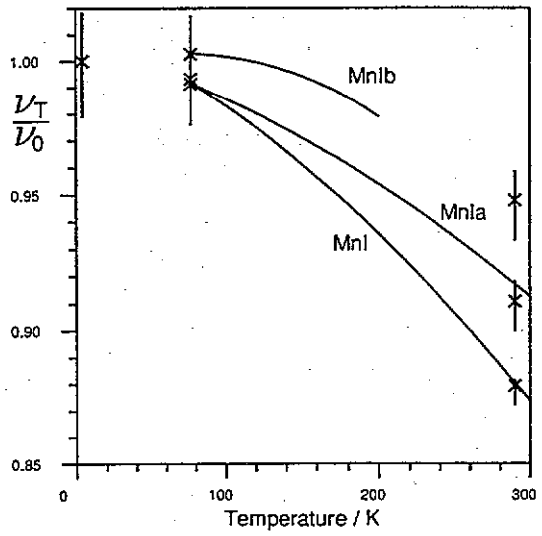

Figure 6. The temperature dependence of the ^{55}Mn NMR of Mn_4N normalized to the value at 4.2 K. The full lines were produced as described in section 4.2. The symbols show measurements made at fixed temperature and typical error bars.

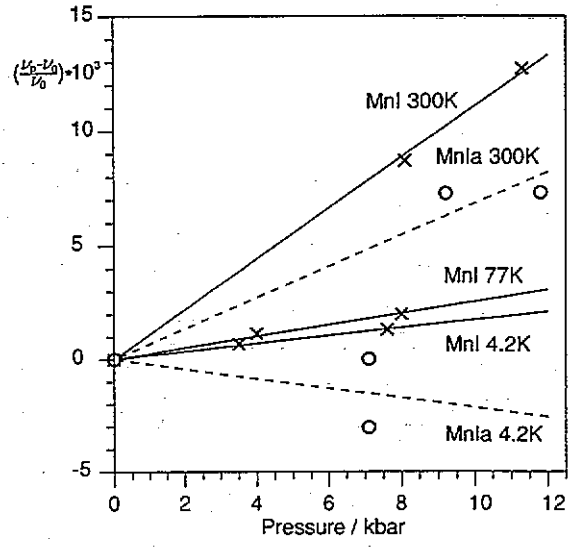

Figure 7. The normalized pressure dependence of the ^{55}Mn NMR at the Mn(I) and Mn(I_a) sites at various temperatures.

of the Mn(II) site is almost constant. (The Néel temperature of Mn is about 750 K [2, 3].)

The pressure dependence of the ^{55}Mn NMR of Mn_4N at various temperatures is shown in figure 7. The surprising feature of these results is that there is an appreciable change in $\partial \ln \nu_T / \partial P$ even between 77 K ($0.10T_N$) and 4.2 K. It has been shown [21] that if it may be assumed that at constant volume the effective field at the nucleus is a function only of T/T_N then the value of $\partial \ln \nu_T / \partial P$ at a given temperature may be related to the value at 0 K by the equation

$$\partial \ln \nu_0 / \partial P = \partial \ln \nu_T / \partial P + (\partial \ln \nu_T / \partial \ln T)\partial \ln T_N / \partial P. \qquad (1)$$

It will be seen from figure 6 that the value of $\partial \ln \nu / \partial \ln T$ for the Mn(I) site of Mn_4N is not negligible even at 77 K. Using equation (1) we deduce that $\partial \ln T_N / \partial P = 5.2$ Mbar^{-1}.

As was remarked in section 3 the calculated value of the effective field at the Mn(I) site (−50 kG) is in surprisingly poor agreement with experiment (table 2). We now show that consistent estimates of the contributions to the effective field are obtained from the pressure dependence of H_I and from the position of the satellite line from the $Mn(I_a)$ site. The established empirical model for the effective magnetic field at a nucleus is to attribute it to a term due to the magnetic moment (H_s) at the site plus a transfer term (H_t) from neighbouring atoms. At Mn(I) therefore

$$H_I = H_s + H_t = \alpha\mu_I + 12\beta\mu_{II}$$

since there are 12 Mn(II) sites around an Mn(I) site, where α and β are constants to be determined. The moment per formula unit may be written

$$\mu = \mu_I + 3\mu_{II}$$

and, neglecting the small pressure dependence of μ_I [15],

$$\partial \ln\sigma/\partial P = \partial \ln\mu/\partial P = (3/\mu)\partial\mu_{II}/\partial P$$

therefore

$$\partial H_I/\partial P = (\mu H_t/3\mu_{II})\partial \ln\sigma/\partial P.$$

Using the values in tables 1–3

$$H_s = -178 \text{ kG} \qquad H_t = +51 \text{ kG}. \tag{2}$$

An alternative calculation of the contributions to H_I may be made using the position of the $Mn(I_a)$ satellite line. An $Mn(I_a)$ site has three Mn(II) nearest neighbours that are also nearest neighbours of the N vacancy, so

$$H_{I_a} = \alpha\mu_I + 9\beta\mu_{II} + 3\beta\mu_{II_a} = H_I + 3\beta(\mu_{II_a} - \mu_{II}).$$

The values of μ_{II} and μ_{II_a} given in table 1 lead to $\beta = 6.0 \text{ kG}\mu_B^{-1}$ and therefore for H_I

$$H_s = -192 \text{ kG} \qquad H_t = +65 \text{ kG}. \tag{3}$$

Since these values are, in view of the approximate nature of the model, in excellent agreement with those deduced from the high-pressure experiments [2], equation (2), we conclude that the large increase in the magnitude of the moment at an Mn(II) site next to an N impurity proposed from the neutron scattering experiments is supported by the present NMR measurements. It should be noted that in deriving equation (2) the value of $\partial \ln\mu_I/\partial P$ was set equal to zero but it is probably small and negative and this would tend to bring the estimated values of H_s and H_t still closer to the values given in (3).

Finally, we consider the value of H_s for the Mn(I) site in terms of contributions proportional to the spin and orbital moments at the site. It is well established that the spin moment leads to a field $\simeq -130 \text{ kG}\mu_B^{-1}$. The value for the orbital moment is less certain but is $\simeq 650 \text{ kG}\mu_B^{-1}$ (see [22] for discussion). Taking the value of H_s to be ~ -185 kG from equations (2) and (3) above leads to moments on the Mn(I) site of

$$\mu_s = 3.45\mu_B \qquad \mu_0 = 0.4\mu_B. \tag{4}$$

The NMR measurements therefore suggest that there is an appreciable orbital moment at the Mn(I) site and hence explain the large discrepancy between the calculations, which only considered the spin moment, and the experimental values of the Mn(I) moment and the effective field. The spin moment shown above is in good agreement with the value calculated by Matar *et al* [12] and Tagawa and Motizuki [13]. The proposed orbital moment at the Mn(I) site would also account for the large anisotropy constant of Mn_4N ($H_A \sim 8$ kG) found by Fruchart *et al* [3]. At present only preliminary, non-converged, ASW calculations have been performed for the orbital moment of Mn_4N [24], and these indicate that the orbital moment is only $\sim 0.03\mu_B$, i.e. an order of magnitude less than suggested by the above analysis, so further work, e.g. magnetic x-ray scattering, is required to clarify the position.

6. Conclusion

The Mn_4N compounds, where M is Fe or Mn, are expanded lattice metals with large moments at the rather isolated M(I) sites and smaller moments at M(II) sites, which are more strongly bonded to N. The present NMR data suggest that Fe_4N is a simple ferromagnet with little or no difference between the pressure dependence of the effective fields at the two Fe sites. The Mn_4N magnetization is more complicated. The basic structure is ferrimagnetic and the increase in the magnitude of the effective field at the Mn(I) site is interpreted as arising from a decrease under pressure of the magnitude of the Mn(II) moment. The pressure measurements, and the value of the effective field at an Mn(I) site next to an N vacancy, support the model, originally proposed from neutron diffraction experiments, in which the magnitude of the moment at an Mn(II) site next to an N vacancy is increased by $1\mu_B$ over the value in the perfect lattice.

Acknowledgments

It is a pleasure to thank Dr R G Graham for his contribution to the early part of this work and the Science and Engineering Research Council for financial support.

References

[1] Takei W J, Heikes R R and Shirane G 1962 *Phys. Rev.* **125** 1893
[2] Mekata M, Haruna J and Takaki H 1966 *J. Phys. Soc. Japan* **21** 2267
[3] Fruchart D, Givord D, Convert P, l'Hértier P and Sénateur J P 1979 *J. Phys. F: Met. Phys.* **9** 2431
[4] Matsuura M 1966 *J. Phys. Soc. Japan* **21** 886
[5] Armitage J G M, Graham R G, Riedi P C, Matar S F and Demazeau G 1991 *High Pressure Res.* **7** 402
[6] Armitage J G M, Graham R G, Lord J S, Riedi P C, Matar S F and Demazeau G 1992 *J. Magn. Magn. Mater.* **104–7** 1935
[7] Andriamandroso D, Fefilatiev L, Demazeau G, Fournès L and Pouchard M 1984 *Mater. Res. Bull.* **19** 1187
[8] Kuhnen C A, de Figueiredo R S, Drago V and da Silva E Z 1992 *J. Magn. Magn. Mater.* **111** 95
[9] Andriamandroso D, Demazeau G, Pouchard M and Hagenmuller P 1984 *J. Solid State Chem.* **54** 54
[10] Mohn P, Schwarz K, Matar S and Demazeau G 1992 *Phys. Rev.* **45** 4000
[11] Matar S F, Demazeau G, Hagenmuller P, Armitage J G M and Riedi P C 1989 *Eur. J. Solid State Inorg. Chem.* T **26** 517
[12] Matar S F, Mohn P, Demazeau G and Siberchicot B 1988 *J. Physique* **49** 1761
[13] Tagawa Y and Motizuki K 1991 *J. Phys.: Condens. Matter* **3** 1753
[14] Ishida S and Kitawatase K 1992 *J. Magn. Magn. Mater.* **104–7** 1933

[15] Siberchicot B and Matar S F 1991 *J. Magn. Magn. Mater.* **101** 419
[16] Armitage J G M, Dumelow T, Riedi P C and Abell J S 1989 *J. Phys.: Condens. Matter* **1** 3987
[17] Dumelow T and Riedi P C 1987 *Hyperfine Interact.* **35** 1061
[18] Armitage J G M, Riedi P C and Abell J S 1990 *J. Phys.: Condens. Matter* **2** 8779
[19] Abe H, Yasuoka H and Hirai A 1966 *J. Phys. Soc. Japan* **21** 77
[20] Barkhuijsen H, de Beer R, Bovée W M J and van Ormondt D 1985 *J. Magn. Res.* **61** 465
[21] Riedi P C 1981 *Phys. Rev.* B **24** 1593
[22] Riedi P C, Dumelow T, Rubinstein M, Prinz G A and Qadri S B 1987 *Phys. Rev.* B **36** 4595
[23] Mohn P 1993 private communication
[24] Matar S F 1993 unpublished